CHAPTER 4

SIMULATION

1. Int. J. Electr. Electron. Engg. Res. Dev., **1 (1)** (2011) 1.
2. Int. J. Electron. Commun. Comp. Engg., **3 (3)** (2012) 362.
3. Int. J. Electr. Electron. Engg. Res., **2 (3)** (2012), 1-11.

4.0 INTRODUCTION

In this chapter various maximum power point tracking (MPPT) methods based on number of sensors required, speed of convergence, ability to perform under noisy and environmentally varying conditions have been simulated and discussed. The stability of maximum peak point without oscillating around the peak has been described. A new hybrid MPPT algorithm has been suggested, which combines the advantages of fractional open circuit voltage, variable step and optimized hill climbing MPPT algorithm.

4.1 SIMULATION OF PERTURB AND OBSERVE (P&O) ALGORITHM

The perturb and observe or hill-climbing MPPT algorithm is based on the fact that, on the voltage-power characteristics, variation of the power against voltage $dP/dV > 0$ on left of the MPP, while on the right, $dP/dV < 0$ as shown in Fig. 4.1. If the operating voltage of the PV array is perturbed in a given direction and $dP/dV > 0$, the perturbation moves the array's operating point toward the MPP. The P&O algorithm is continued to perturb the PV array voltage in the same direction. If $dP/dV < 0$, then the change in operating point moves the PV array operating point away from the MPP, and the P&O algorithm reverses the direction of the perturbation.

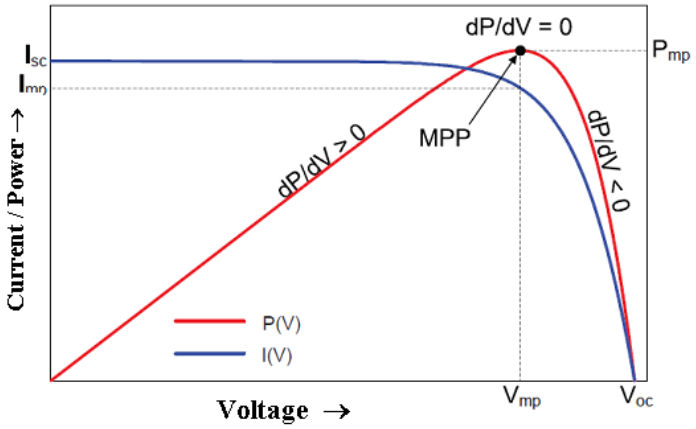

Fig. 4.1 Sign of dP/dV at different positions on the power characteristics of a PV module.

The flow chart of P&O algorithm is as shown in Fig. 4.2. The main advantage of the P&O method is that it is easy to implement, it has low computational complexity and it is applicable for most of the PV systems. It does not require any information about the PV array except the measured voltage. Because of this, the P&O is one of the most-often used MPPT method nowadays. The two main problems of the P&O are the

oscillations around the MPP in steady state conditions, and poor tracking (possibly in the wrong direction, away from MPP) under rapidly-changing irradiations. In order to evaluate the performance of P&O algorithm, a commercially available PV module with a peak output power of 39 W_p watts, short circuit current (I_{sc}) of 2.6 A and open circuit Voltage (V_{op}) of 21 V under standard test conditions of irradiance (G = 1000 W / m^2) and nominal operating cell temperature (NOCT) of 25^oC was simulated using MATLAB.

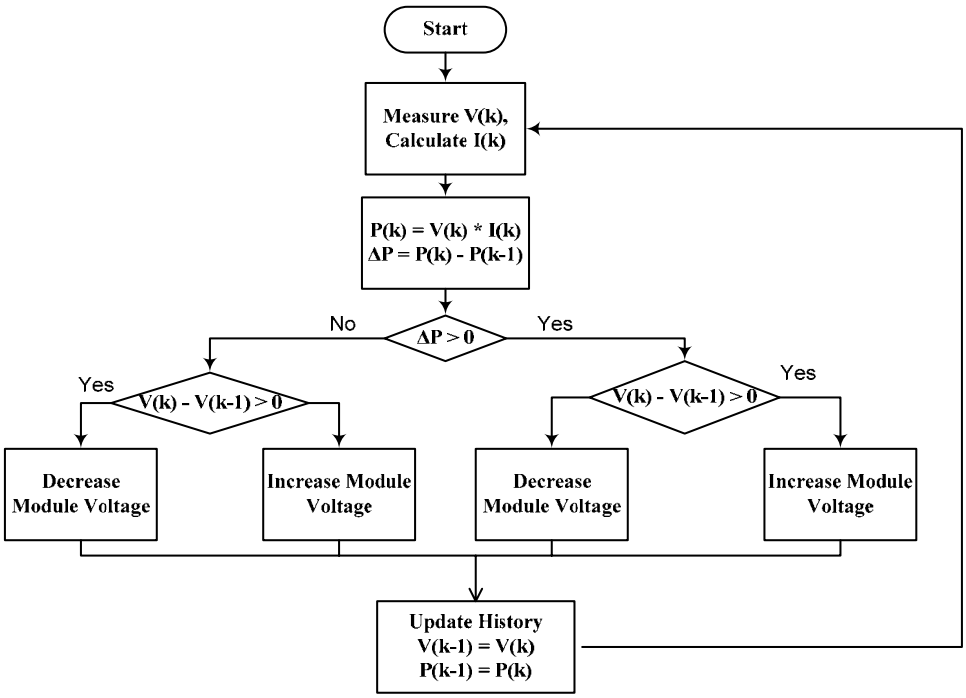

Fig. 4.2 The flowchart of the P&O algorithm.

The mathematical model of PV array has already been explained in Chapter 3. The graphical user interface (GUI), performance parameters of the solar module and the results obtained are shown in Fig. 4.3. Parameters for the implementation of MATLAB programme of PV module are given below:

- **Inputs for GUI interface (Refer Fig. 4.3 (c)**
  - Short circuit current (I_{SC}) = 2.6 A
  - Open circuit voltage (V_{OC}) = 21 V
  - Irradiance (G) (1 = 1000 W / m^2) = 1
- **Constants for initialization**
  - k = Boltzmann constant = 1.381×10^{-23} J/K
  - q = Electron charge = 1.602×10^{-19} J

- n = Diode ideality factor
- V_T = Thermal Voltage at 300 ^oK= 25.9 mV
- Ns = Number of solar cells in series.
- FS_{max}= Fixed Step size

- **Method:** (Refer Fig. 4.3 (a))
  - Measure V(k)
  - Vary temperature from 0 ^oC to 75 ^oC in steps of 25^oC
  - For each value of Temperature calculate
  - Calculate Rs using Eq. 3.26 and Eq. 3.27
  - Calculate Ia(k) using Eq. 3.38
  - Calculate Pa(k) = Ia(k) x Va(k)
  - Find maximum power point
- **Output Files**
  - Plot (Va, Ia)
  - Plot (Pa, Va)

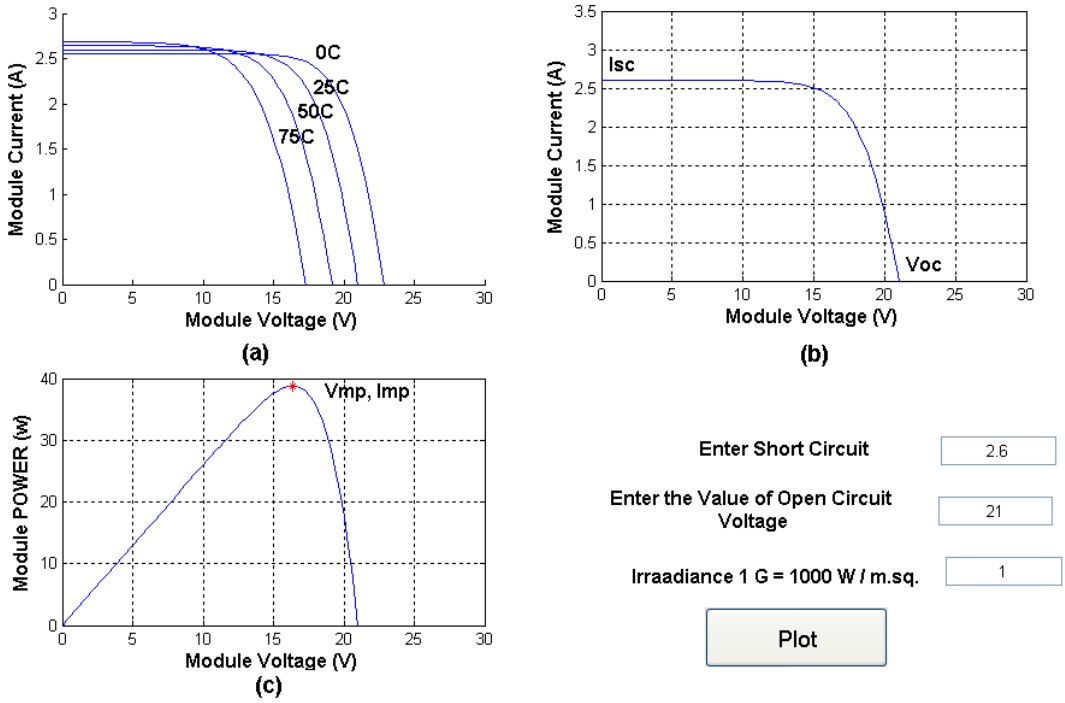

Fig. 4.3 Output of a MATLAB-GUI showing (a) Variation of V-I with respect to temperature. (b) V-I curve of PV module under standard test conditions (c) Power curve with respect to module voltage under standard test conditions.

The simulations have been done for various values of step size. The simulation for a MPP Tracking for a step size of 0.5 V and input irradiance of a trapezoidal pattern are shown in Fig. 4.4. The MPP at 200 W/m^2, 400 W/m^2, 600 W/m^2, 800 W/m^2, and 1000 W/m^2 insolation levels are marked prominently to confirm the accuracy of tracking. The implementation of MATLAB programme for P&O algorithm is stated below:

- **Input for GUI interface**
  - I_{SC}, V_{OC},
  - Load Irradiance .dat file.
- **Constants for initialization**
  - K, q, n, V_T, Ns, FS_{max}
- **Method:** (Refer Fig. 4.2)
  - Insert "tic" and "toc" functions of MATLAB for time measurement of transient response to step function.
  - Calculate Rs, Ia and Pa
  - ΔP = Pa_new – Pa (ΔP(k) = P(k) – P(k-1))
  - ΔV= Va_new – Va (ΔV(k) = V(k) – V(k-1))
  - Va_new = Va + FS_{max} to increase reference Voltage
  - Va_new = Va - FS_{max} to decrease reference Voltage
- **Output Files**
  - Va_new_array [ ]; Ia_new_array [ ]; Pa_new_array [ ]
  - Plot (Pa,Va) (refer Fig. 4.4)
  - Create Outpower.mat file

4.2 SIMULATION OF INCREMENTAL ALGORITHM

The Incremental Conductance (INC) algorithm is similar to P & O algorithm. It uses instantaneous ratio of current and voltage (I/V) and incremental conductance dI/dV for obtaining the MPP. The mathematical relations can be written as:

$$\frac{dP}{dV} = \frac{d(VI)}{dV} = V\frac{dI}{dV} + I, \tag{4.1}$$

$$\left.\frac{dP}{dV}\right|_{\substack{I=I_{mp}\\V=V_{mp}}} = 0, \tag{4.2}$$

$$\text{and} \qquad \left.\frac{dI}{dV}\right|_{\substack{I=I_{mp}\\V=V_{mp}}} = -\frac{I_{mp}}{V_{mp}} \tag{4.3}$$

where V_{mp} is the MPP voltage of the module and I_{mp} is the MPP current of the module.

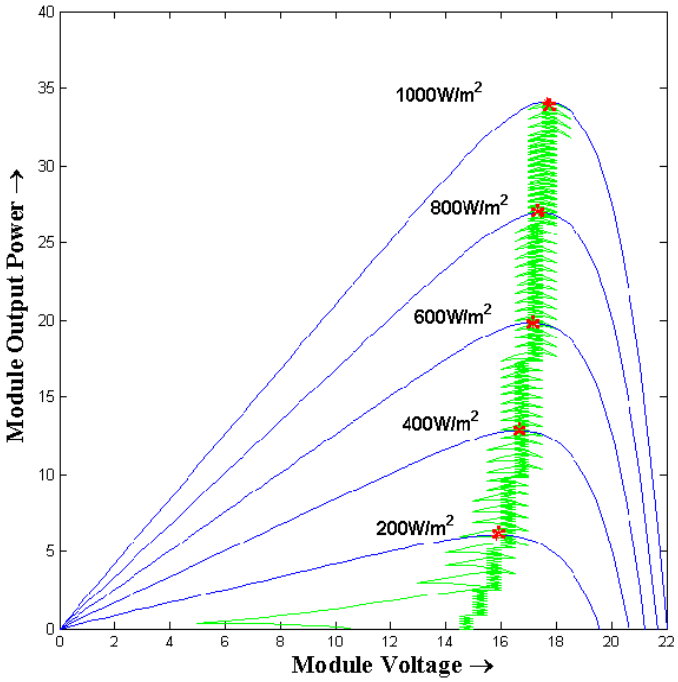

Fig. 4.4 Tracking of P&O MPPT method.

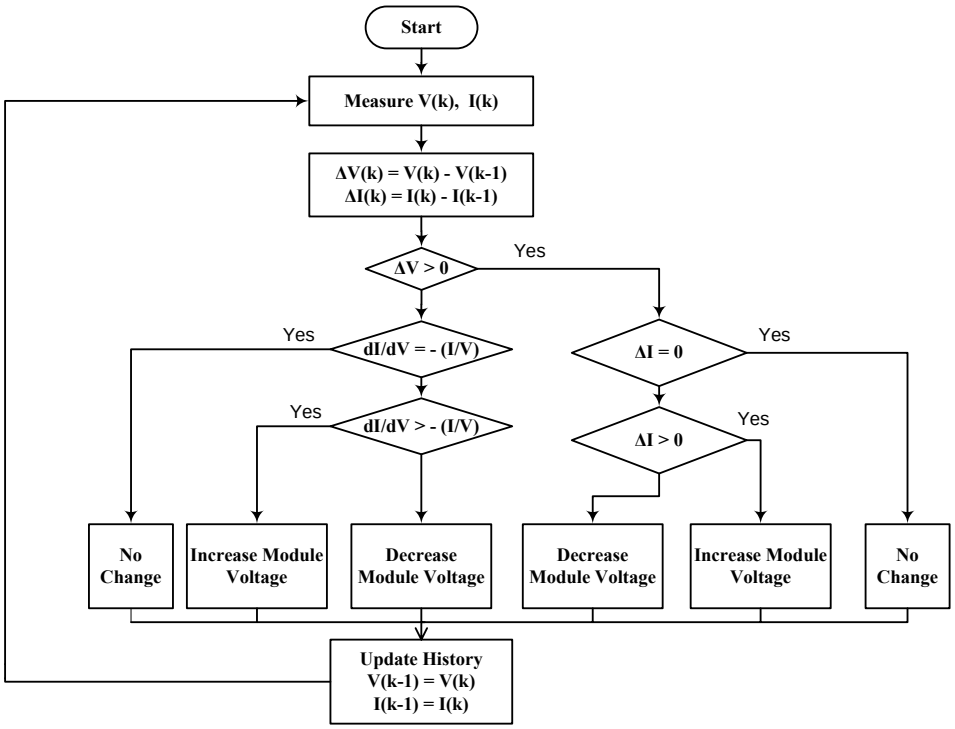

Fig. 4.5 Flow chart of incremental algorithm.

The MPPT is tracked using Eq. (4.2). A threshold error is normally allowed to make a tradeoff between the convergence speed and the allowable oscillations at the peak point limiting the sensitivity of the tracker. The flow chart of the incremental conductance algorithm (INC) is shown in Fig. 4.5. It has the disadvantage of tracking in wrong direction during rapidly-changing irradiations and low irradiance conditions. The simulation for a MPP tracking for a step size of 0.5 V and a threshold acceptable error of 0.002 for an input irradiance of a trapezoidal pattern is shown in Fig. 4.6.

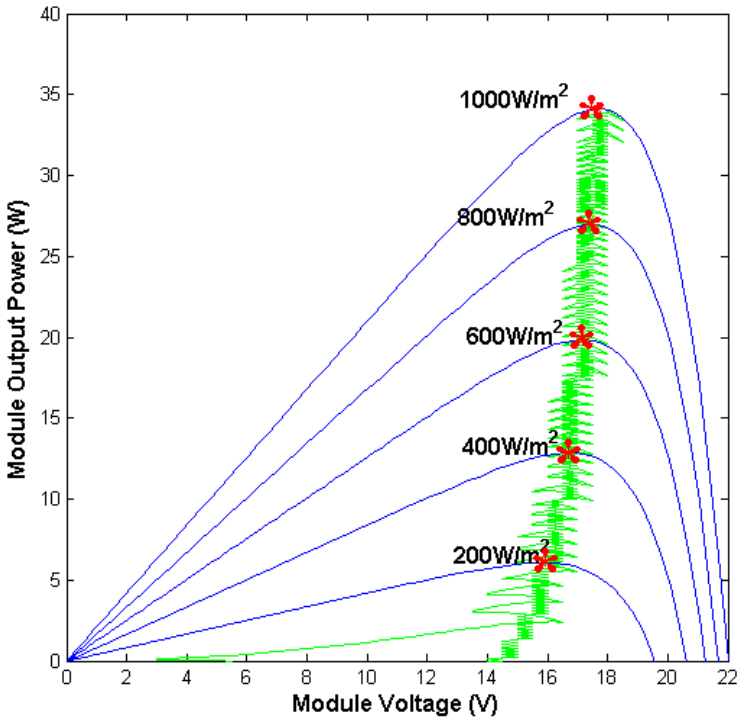

Fig. 4.6 Tracking of incremental MPPT method.

The peak points are highlighted with an asterisk sign on a reference power curve at irradiance values of 200 W/m^2, 400 W/m^2, 600 W/m^2, 800 W/m^2 and 1000 W/m^2. Several researchers (Hohm and Ropp 2003, Hua and Shen 1998) have compared the above algorithms (P&O, INC and FCV) and it has been observed that in high irradiation conditions, the INC produces the highest efficiency. On the other hand, if the irradiance decreases, the efficiency of the INC is also decreased and further deteriorates at very low irradiance levels. The efficiency of the P&O also decreases with less irradiation, but it tracks the low irradiance levels. The fractional constant voltage (FCV) method is generally considered the least efficient, but as the irradiance decreases, it shows

improving performance, higher than both the P&O and INC. Because of this property, it is often used in combination with one of the hill-climbing methods.

4.3 SIMULATION OF PROPOSED HYBRID ALGORITHM

The power drawn from the PV array with a lager step size contributes to faster dynamics but excessive steady state oscillations, results in a comparatively low efficiency. If iteration step size is small, the power drawn from the PV module has slower dynamics. This problem can be removed by using the second algorithm, i.e., incremental MPPT with variable step size. In this algorithm, if the operating point is far from MPP, it increases the step size which enables a fast tracking ability. If the operating point is near to the MPP, the step size becomes very small and the oscillation is reduced contributing to a higher efficiency. Variable step size incremental MPPT algorithm effectively improves the MPPT speed and accuracy simultaneously.

The main advantage of incremental algorithm over the P&O method is its fast power tracking process. However, it has the disadvantage of possible output instability due to the use of derivative algorithm. Also the differentiation process under low levels of insolation becomes difficult and results are unsatisfactory. The rapidly changing conditions are tracked by an optimized hill climbing MPPT method dP-P&O (Dezso et al. 2008). The algorithm separates the effects of the irradiation change from the effect of the tracker's perturbation by performing an additional measurement in the middle of the MPPT sampling period as shown in Fig. 4.7. This information is optimized in tracking according to the irradiation change. The change in power between P_x and P_k reflects the change in power due to the environmental changes, as no action has been made by the MPPT. The difference between P_x and P_{k-1} (dP_{PI}) contains the change in power caused by the perturbation of the MPPT plus the irradiation change, if the rate of change in the irradiation is constant over one sampling period of the MPPT. The difference between the two consecutive measurements of power is used to determine the next perturbation direction. This is the extra computational load as compared to classical P&O method, if the change in power due to irradiation $|dP_I|$ is smaller than the change of power due to the MPPT perturbation $|dP|$. It is considered to be a slowly varying condition and the system will automatically use the basic dP-P&O algorithm with small increment values to reduce oscillations around the MPP.

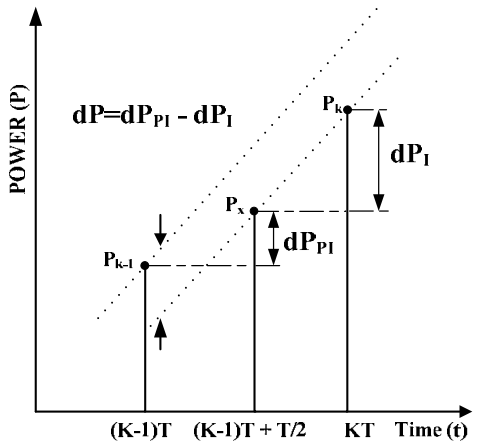

Fig. 4.7 Measurement of the power between two MPPT sampling instances.

The knowledge of the direction of the irradiation change enables the MPPT to use different optimized tracking schemes for the different cases of increasing, decreasing, or steady irradiance. When the irradiance is changing rapidly, this leads to faster and better tracking, while in steady-state conditions it leads to lower oscillations around the MPP. The proposed hybrid algorithm combines the advantages of all the above three algorithms along with variable step algorithm for faster convergence and reduced oscillations at the peak point. The flow chart of the proposed hybrid algorithm is shown in Fig. 4.8.

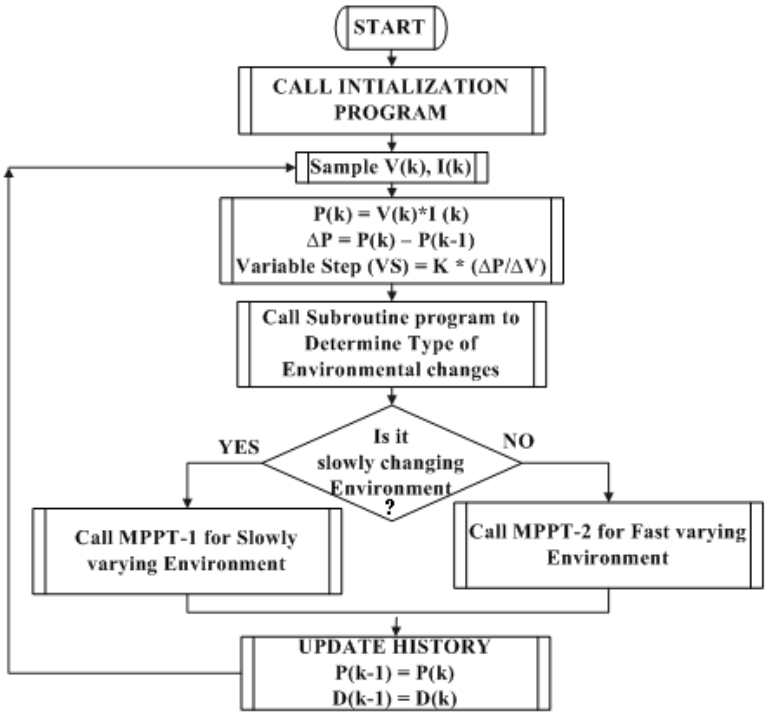

Fig. 4.8 Flow chart of the proposed hybrid algorithm.

The first step is the initialization of program as shown in Fig. 4.9. This will set the PV arrays operating voltage point to 78% of the measured value of the open circuit voltage which was decided from the V-I curve tracer for various operating temperatures.

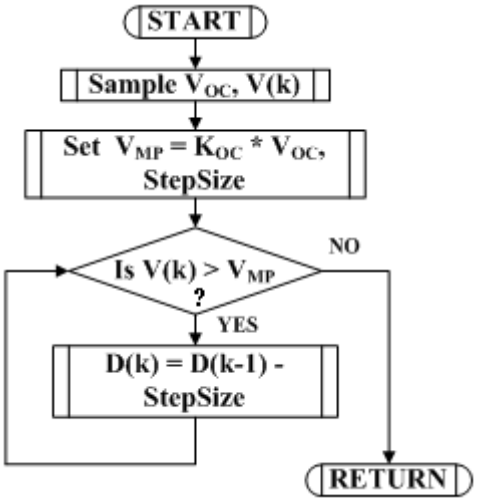

Fig. 4.9 The flow chart of initialization program.

The P&O algorithm does not use the exact power out of the solar panel, but a difference of the proportional power. The amount the power changed has no effect on the algorithm. For this reason, the exact power out of the solar panel is not required, which allows us to use the linear relationship of the PWM's duty cycle and the solar panels current. The proportional power out of the solar panel is calculated by multiplying the voltage of the solar panel by the duty cycle of the PWM. A variable step has been used to track the peak point quickly and accurately. Different types of environmental changes have been observed and two different algorithms have been initiated for slowly varying environmental conditions and fast varying environmental conditions.

The change in the power ($\Delta P = P(k) - P(k-1)$) is calculated by the measurement of V(k), V(k-1) and the values of I(k) and I(k-1). In order to avoid oscillations at the MPP, no actions are initiated if the change in power is within the threshold limit of $|\varepsilon|$. The size of the variable step is decided by the ratio of $\Delta P/\Delta V$, i.e., if the change in power is more than the variable step, the size will be larger or vice versa. The type of environmental variations is calculated using dP-PO algorithm. If the change in power due to irradiation ($|dP_I|$) is smaller than the change of power due to the MPPT perturbation ($|dP|$) as shown in Fig. 4.10 (a), it is considered to be a slowly changing

condition and the system will use the basic variable step P&O algorithm (MPPT1) with small increment values to reduce oscillations around the MPP as shown in Fig. 4.10 (b).

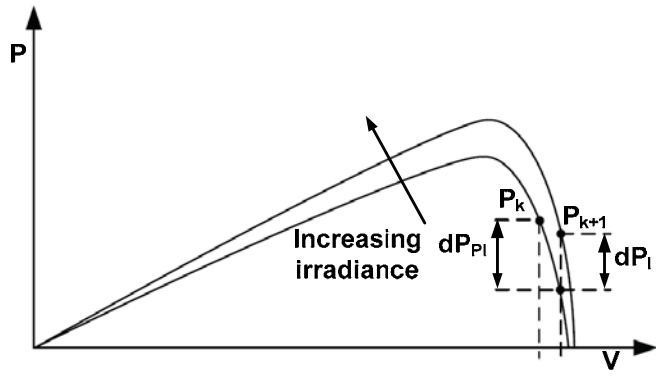

Fig. 4.10 (a) Power vs voltage curve for $|dP_{PI}| > |dP_I|$.

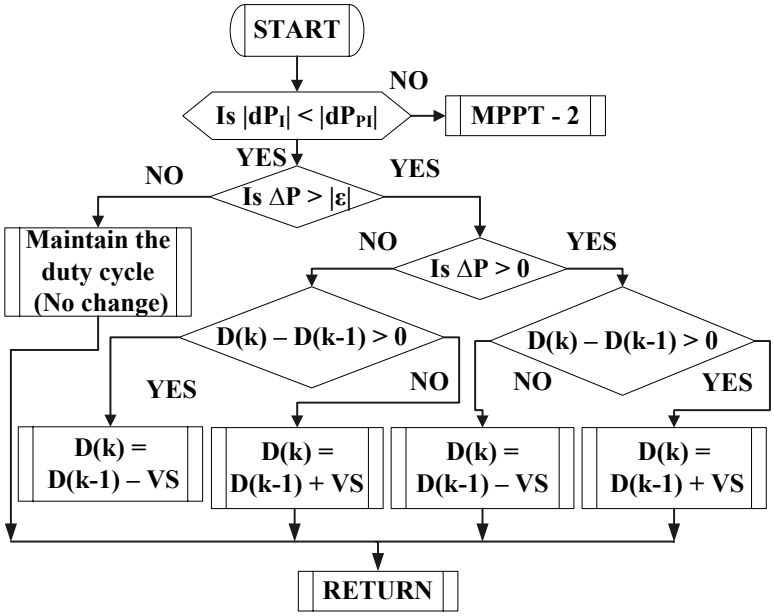

Fig. 4.10 (b) Flow chart of slowly varying environment conditions (MPPT1).

If the change in power due to irradiation ($|dP_I|$) is larger than the change of power due to the MPPT perturbation ($|dP|$) as shown in Fig. 4.11 (a), then it is considered as a fast changing condition. The system will use the variable step P&O algorithm MPPT2 with smaller or larger increment values to reach the MPP quickly as shown in Fig. 4.11 (b). In case of rapidly changing irradiation is detected by dP_I, the MPPT increases or decreases the duty cycle frequently both in magnitude and direction. This causes a reduction of power dP leading to error in direction of protuberance. The direction of the perturbation is not changed till the threshold is reached, thus reducing the number of false changeover.

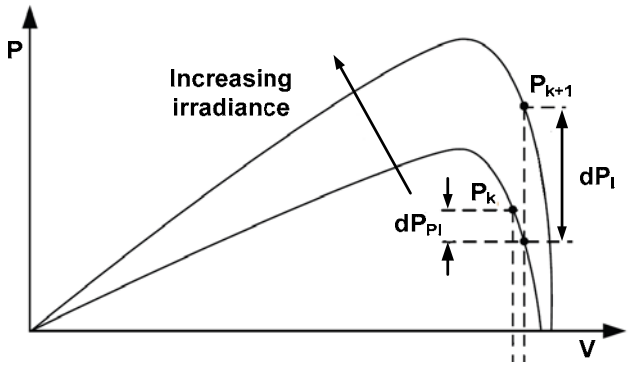

Fig. 4.11 (a) Power vs voltage curve for $|dP_{PI}| < |dP_I|$.

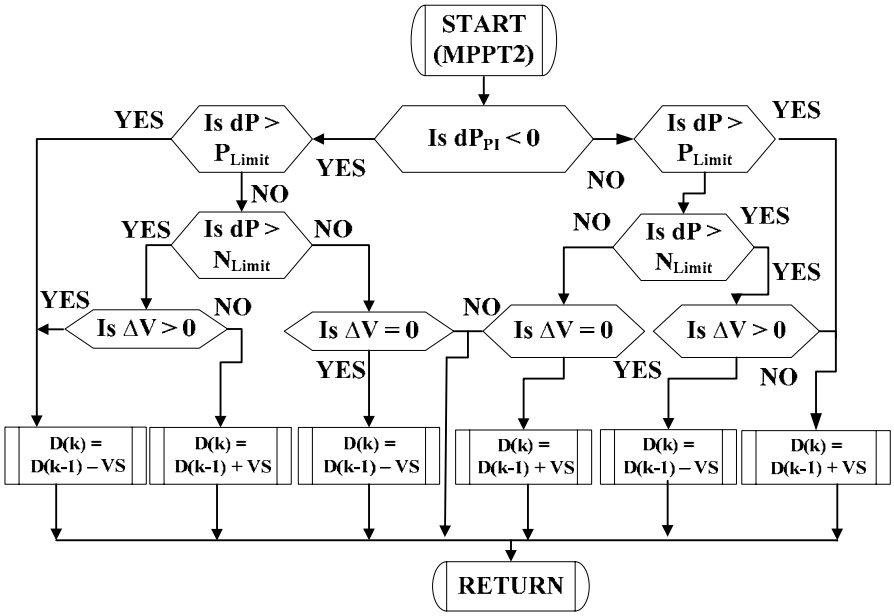

Fig. 4.11 (b) Flow chart of fast varying environmental conditions (MPPT2).

Implementation of MATLAB programme for proposed MPPT algorithm is as given below:

- **Input for GUI Interface**
  - I_{SC}, V_{OC},
  - Load irradiance .dat file.
- **Constants for initialization**
  - K, q, n, V_T , Ns, FSmax,
  - Acceptable Power variations at steady state = ε
  - Positive Tresh hold = P_{Limit}
  - Negative Thresh hold = N_{Limit}

- **Method: (Refer Fig. 4.7 to Fig. 4.10)**
  - Insert "tic" and "toc" functions of MATLAB for time measurement of transient response to step function.
  - Calculate Rs, Ia, Pa, ΔP, ΔV,
  - Calculate Scaling factor and limit it to $K < FS_{max} / \left|\frac{\Delta P}{\Delta V}\right|_{FS_{max}}$
  - Calculate Variable Step Size $VS = K\left|\frac{\Delta P}{\Delta V}\right|$ and
  - Va_new = Va + VS to increase ref. Voltage
  - Va_new = Va - VS to decrease ref. Voltage
  - Execute MPPT1 (Fig. 4.10 (a)), if $|dP_I| < |dP_{PI}|$ **(**Fig. 4.10 (b)**)**
  - Execute MPPT2 (Fig. 4.11 (a)), if $|dP_I| \geq |dP_{PI}|$ (Fig. 4.11 (b))
  - Repeat for complete irradiance data.
- **Output Files**
  - Va_new_array [ ]
  - Ia_new_array [ ]
  - Pa_new_array []
  - Plot (Pa,Va)
  - Create Outpower.mat file

4.4 ANALYSIS OF THE PROPOSED HYBRID MPPT ALGORITHM

Irradiation can change quickly due to weather conditions or passing clouds. In order to evaluate and validate the performance of the proposed system, three test pattern signals were simulated using MATLAB taking into consideration the guide lines shown in Table 4.1 (Bletterie et al. 2006).

Table 4.1 Classification of irradiation changes

Sl. No.	Description	Time Scale (seconds)	Largest Realistic variation (W/m^2)
1	Very Fast	1	27
2	Fast	5	103
3	Slow	30	441

In order to optimize the value of step size, simulations were carried for staircase type input variance. The time response characteristic for P&O, INC and the proposed

hybrid algorithm are shown in Fig. 4.12 and Fig. 4.13, respectively for different step sizes of 1.5, 2.5 and variable step size were simulated using MATLAB. When the step size is small (1.5 V), both the P&O and incremental MPPT algorithms reach the MPP slowly as shown in Fig. 4.12 as compared to bigger steps (2.5 V) as shown in Fig. 4.13. However, the oscillations at the peak point is more when the step size is increased leading to power losses. In the proposed hybrid algorithm due to the combination of the fractional volatge method and the variable step method, the MPP is reached faster because of the larger and variable step size for larger changes and the oscillations are reduced because of the smaller steps of 0.1 V at MPP.

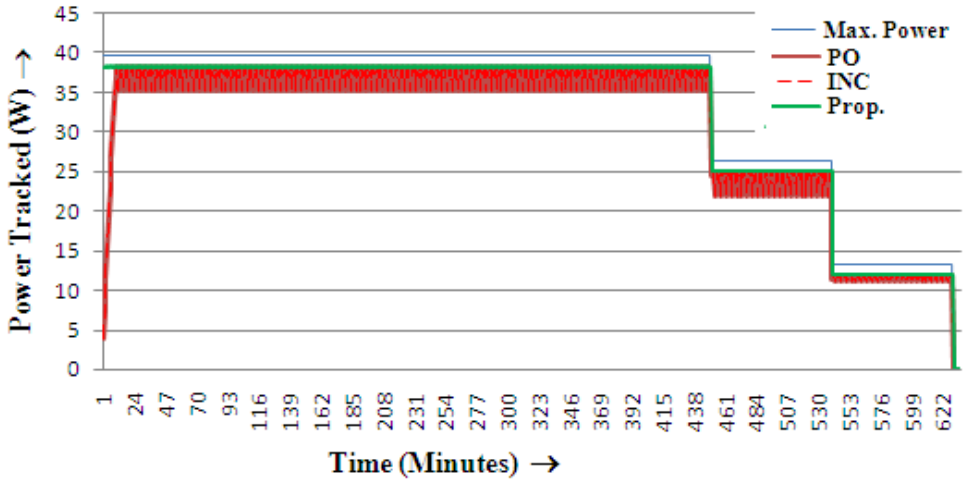

Fig. 4.12 Comparison of a tracking response for a fast changing irradiance for step size of 1.5 V.

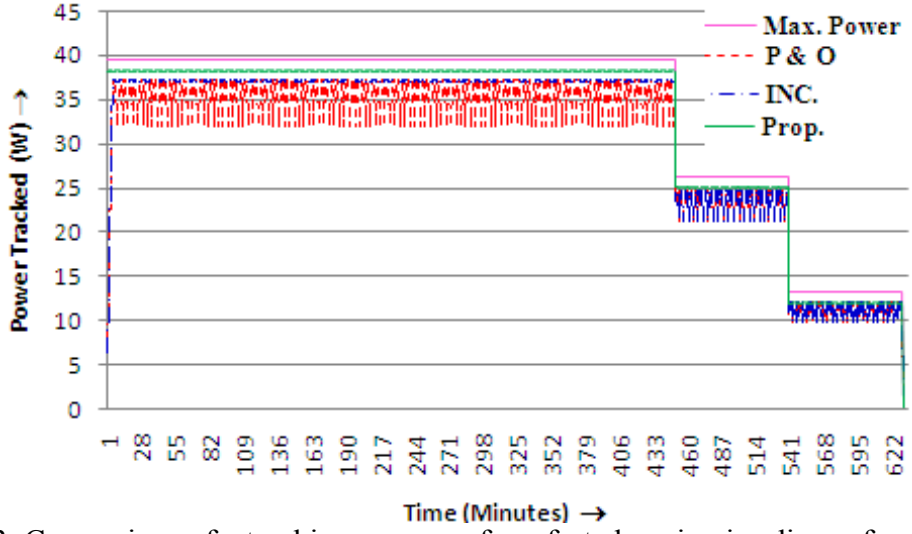

Fig. 4.13 Comparison of a tracking response for a fast changing irradiance for step size of 2.5 V.

The P&O and incremental algorithm are very unstable for low irradiation level because of the optimized large step and differential nature of algorithms, respectively. In the proposed algorithm because of the smaller steps, the MPPT is stable at low irradiance. The improvement in the proposed algorithm is observed for very fast, fast and slow changing environment in terms of improved time response and reduced oscilltaion under steady state response.

In the proposed algorithm if $dP_{PI} > dP_I$, the MPPT is able to determine the correct direction of pertubance changes. The output response for slowly changing environment is shown in Fig. 4.14 for P&O, incremental and the proposed hybrid algorithm. On the other hand, if $dP_{PI} < dP_I$, the MPPT is unable to determine the correct direction of tracking, In order to avoid the wrong direction of tracking, the change in direction is done only when the change is greater than the positive (P_{Limit}) and negative (N_{Limit}) threshold limits. The variable step size which is directly proportional the power change is used to reach the MPP quickly.

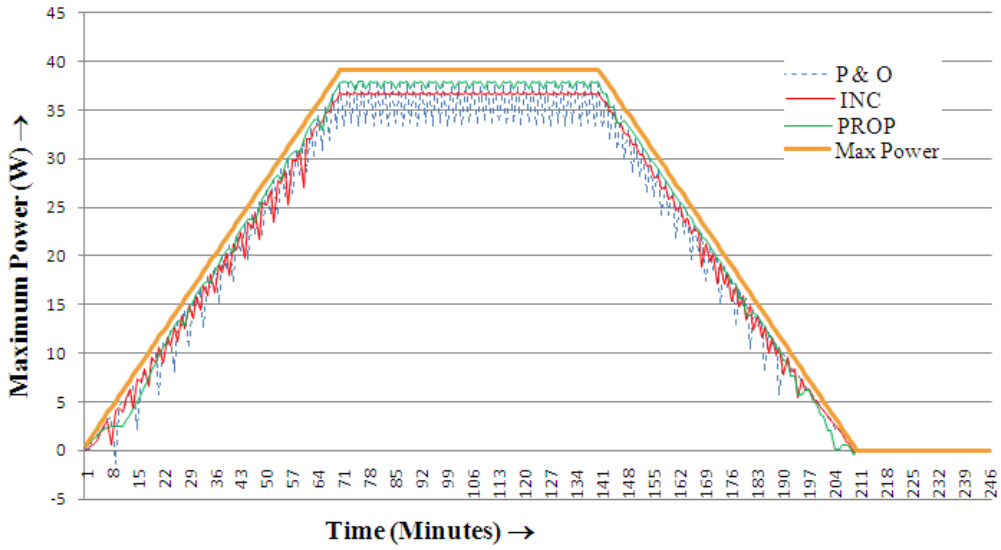

Fig. 4.14 Comparison of a tracking response for slowly changing irradiance for step size of 1.5 V.

The simulation results for V-I characteristics and the power–voltage characteristics were validated using a setup shown in Fig. 4.15 (Ryo et al. 2003).

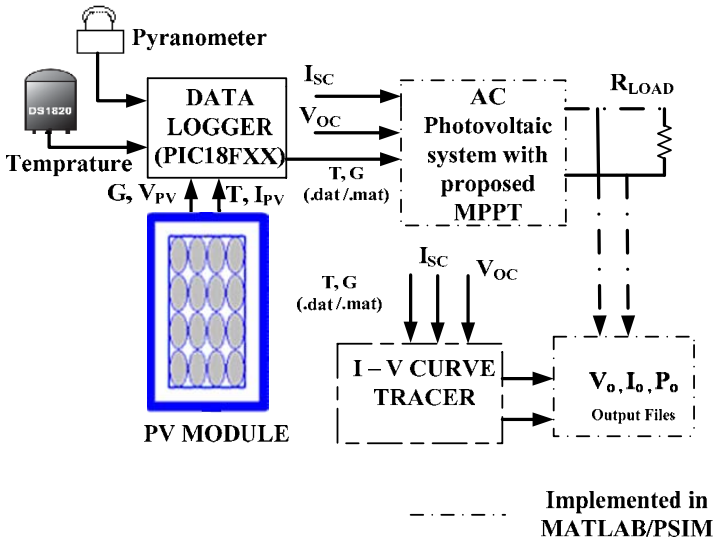

Fig. 4.15 Experimental setup for V-I curve tracer.

The data of irradiance (G), temperature (T), voltage and current of PV module have been collected at the interval of one minute for one day on a memory card using PIC18F722 microcontroller board as shown in Fig. 4.15. Further, the data of G and T have been given to the AC photovoltaic system with proposed MPPT in .dat format to evaluate the performance of the proposed MPPT system.

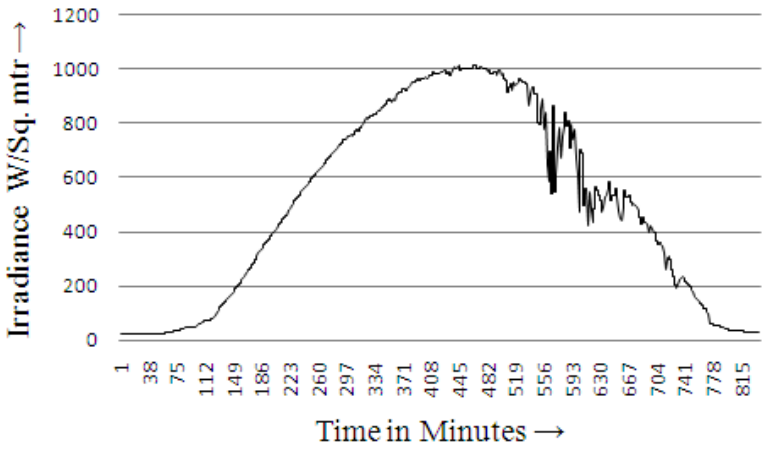

Fig. 4.16 One day insolation values measured at city of Alandi, Pune, India.

The irradiance data of one day, as shown in Fig. 4.16 was given as input to proposed MPPT algorithm and the output power for four algorithms was evaluated. The observations have been summarized in Table 4.2.

$$\left[\sum P_{max}[n]\right]_{Average} = \left[\sum_{Total\ \ time} [I_m[n] \times V_m[n]]\right] \Big/ [Total \quad time] \qquad (4.4)$$

Table 4.2 Comparison of performance parameters of various MPPT algorithms

Sl. No	Parameter	FCV	P & O Algorithm	Incremental Algorithm	Variable Step Incremental Algorithm	Proposed Hybrid MPPT Algorithm
1	Average power for same irradiance test pattern (Maximum = 17.49 W)	14.51 W	15.59 W	16.09 W	16.31 W	16.79 W
2	Increase in Avg. output Power as Compared to Fractional Open-Circuit Voltage (%)	Not Applicable	7.44 %	9.82 %	11.03 %	13.58 %
3	Response Time at start (in ms)	19.77	159.56	119.48	74.35	19.78

It is observed from the Table 4.2 that the proposed algorithm shown in column-7 has an improvement of 13.05 %, 6.14 %, 3.62 % and 2.55 % in average output power (row-2) as compared to fractional voltage (FCV), P&O, incremental conductance and variable step incremental conductance MPPT algorithms, respectively. The response time of the proposed algorithm at start (row-4, column-7) is almost equal to the response time of FCV (row-4, column-3). The overall efficiency calculated from the data of Table 4.2 (row-2 and columns 2 and 7) of the system has been found to be 96.41% (Goudar et al. 2011c). The performance of P&O, INC and the proposed for real time irradiance with a fixed step sizes of 1.0 for P&O and INC algorithm and variable step size for the proposed MPPT algorithm is shown in Fig. 4.17. It is also observed that the performance of P&O, incremental conductence algorithm is varying at low irradiannce because of the instability due to larger step size levels. The proposed algorithm also gives better performance at low irradinace. This is also one of the reasons for improved performance of the proposed MPPT algorithm.

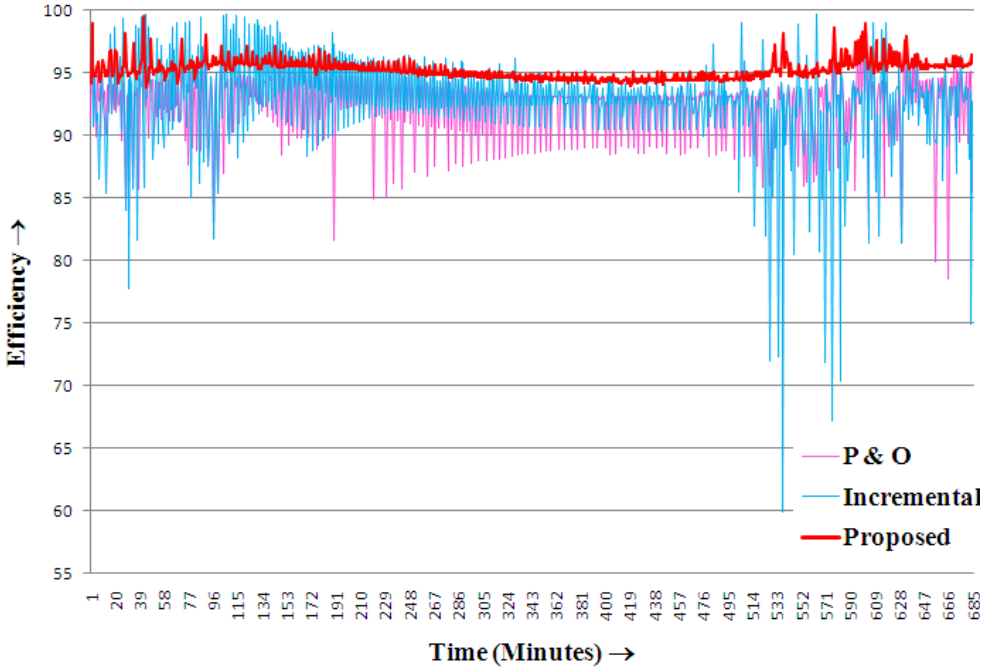

Fig. 4.17 Comparison of a tracking efficiency for P&O, incremental and proposed hybrid algorithm.

4.5 SIMULATION OF AN INVERTER

PSIM software has been used to simulate the inverter circuit. The schematic of the inverter circuit is shown in Fig. 4.18.

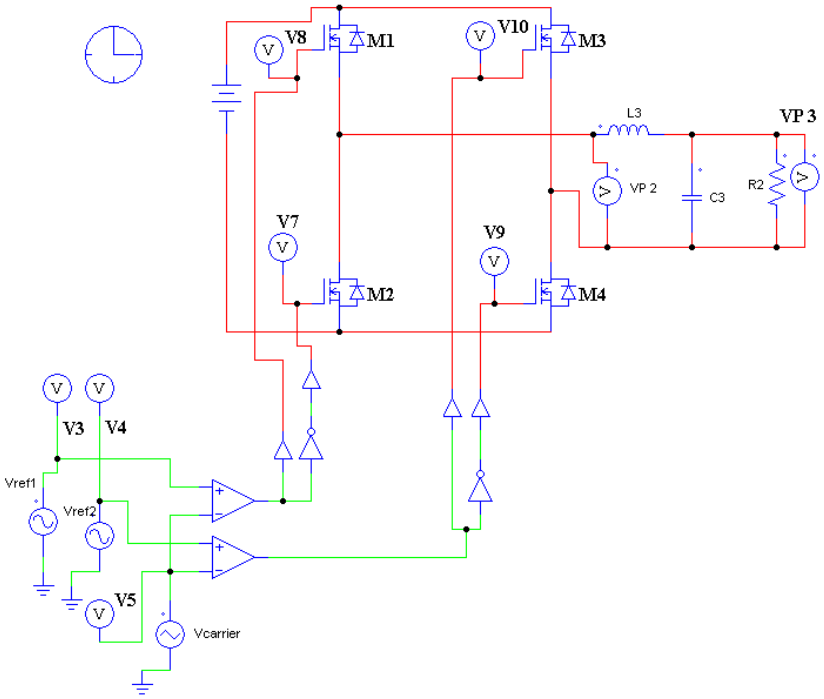

Fig. 4.18 Circuit used for simulating the inverter.

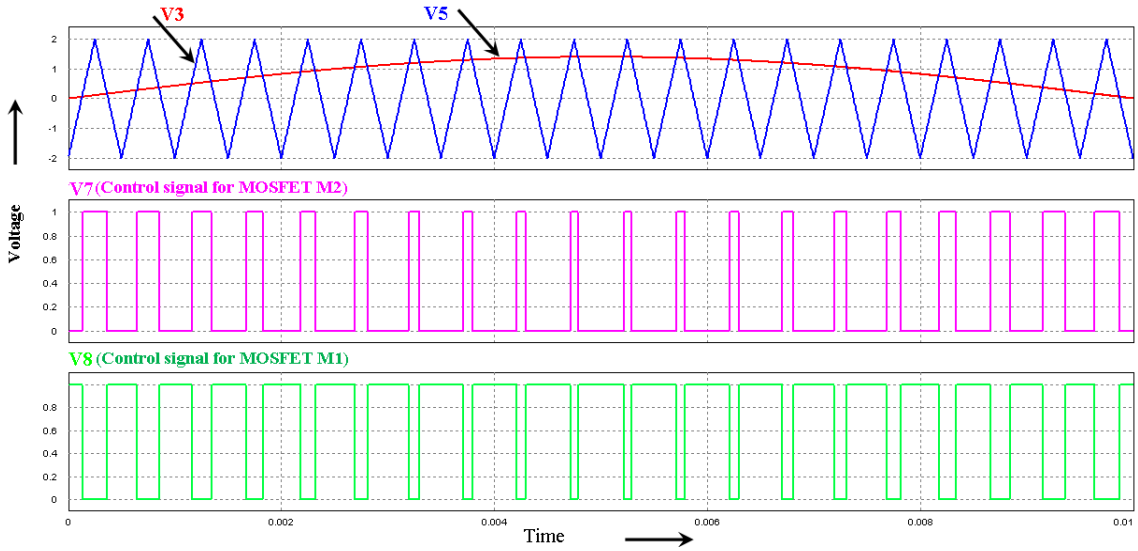

Fig. 4.19 Control signals at the gate of MOSFET 1 and MOSFET 2.

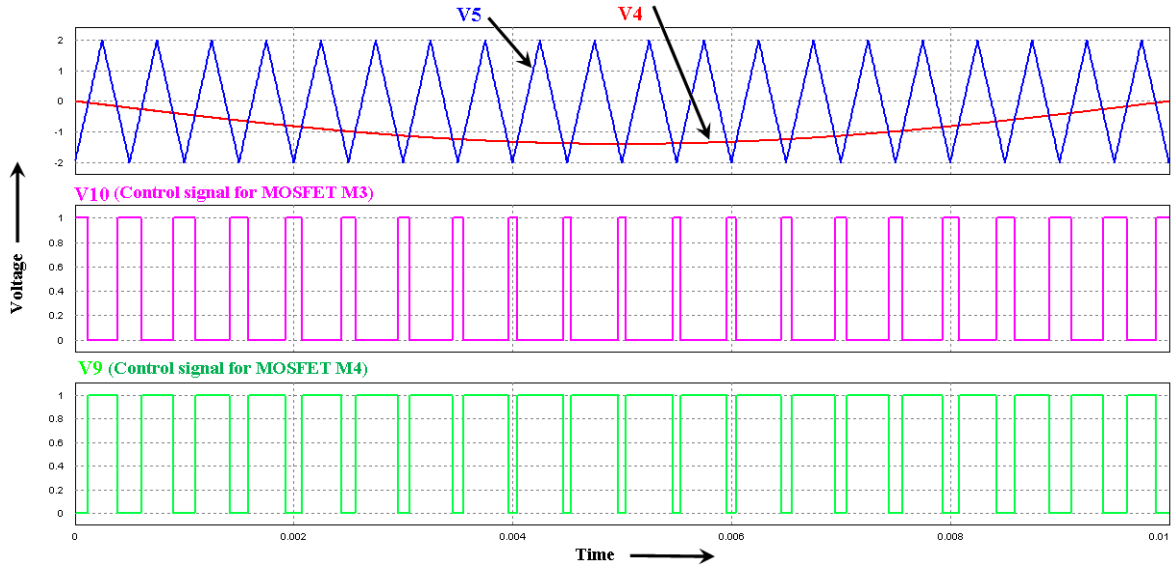

Fig. 4.20 Control signals at the gate of MOSFET 3 and MOSFET 4.

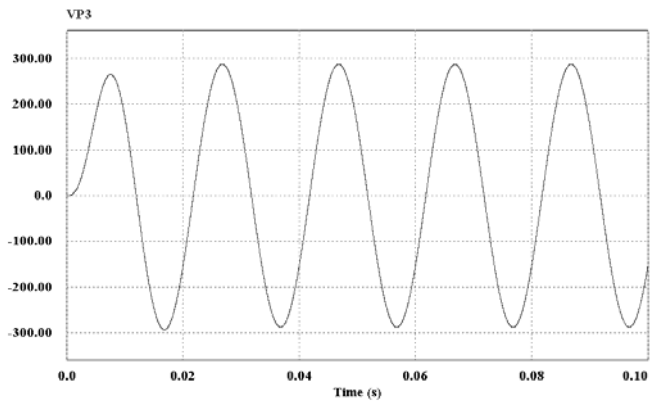

Fig. 4.21 Inverter output after filter.

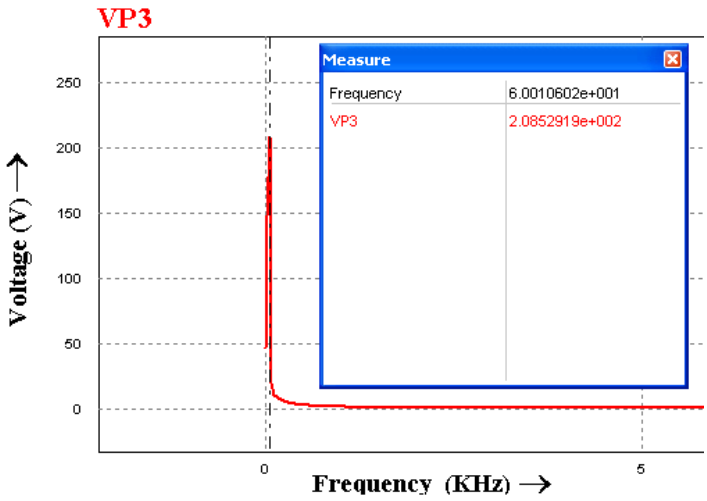

Fig. 4.22 FFT of a inverter output with filter.

4.6 PARTIAL SHADING

When PV modules are connected in series and subjected to partial shading conditions, the resultant output power is different from the algebraic sum of the two individual output power. This is because of the local multiple maxima and minima as explained and simulated in Section 3.2.3. Two PV modules, PV1 and PV2, with I_{SC} of 2.6 A and peak output power of 39 W_P are connected in series and the partial shading effect is created in simulation. The irradiance of 100% is given to PV1 and 50% to PV2. The simulation in PSIM has been done with common MPPT Gating Block as shown in Fig. 4.23 (a). The PSIM simulation is repeated with same partial shading conditions but

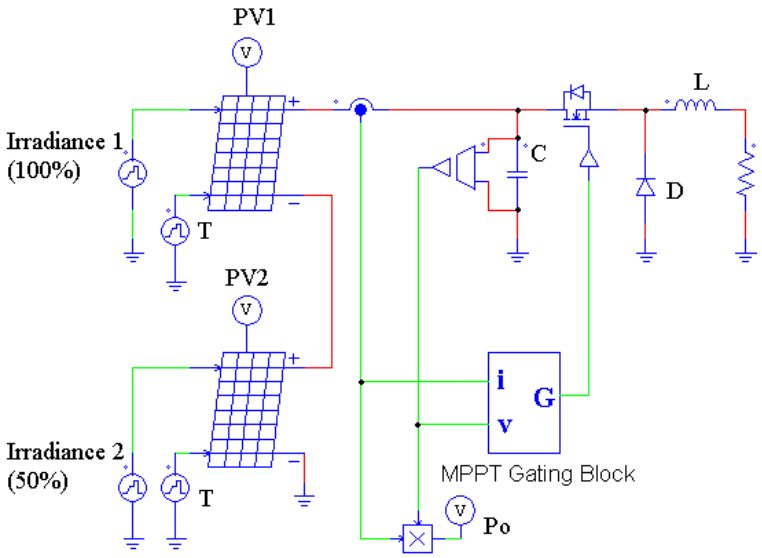

Fig. 4.23 (a) Two PV modules connected in series with uneven irradiance and common MPPT block.

with independent MPPT Gating Block for each PV module as shown in Fig. 4.23 (b). The simulations have been repeated for P&O, variable step incremental algorithm and the proposed MPPT algorithm. The observations and findings are summarized in Table 4.3. From this table, it is observed that in the proposed MPPT algorithm there is an improvement of average output power of 12.36% , 3.4% and 0.29 % with respect to partial shading, P&O and variable step incremental MPPT algorithm, respectively.

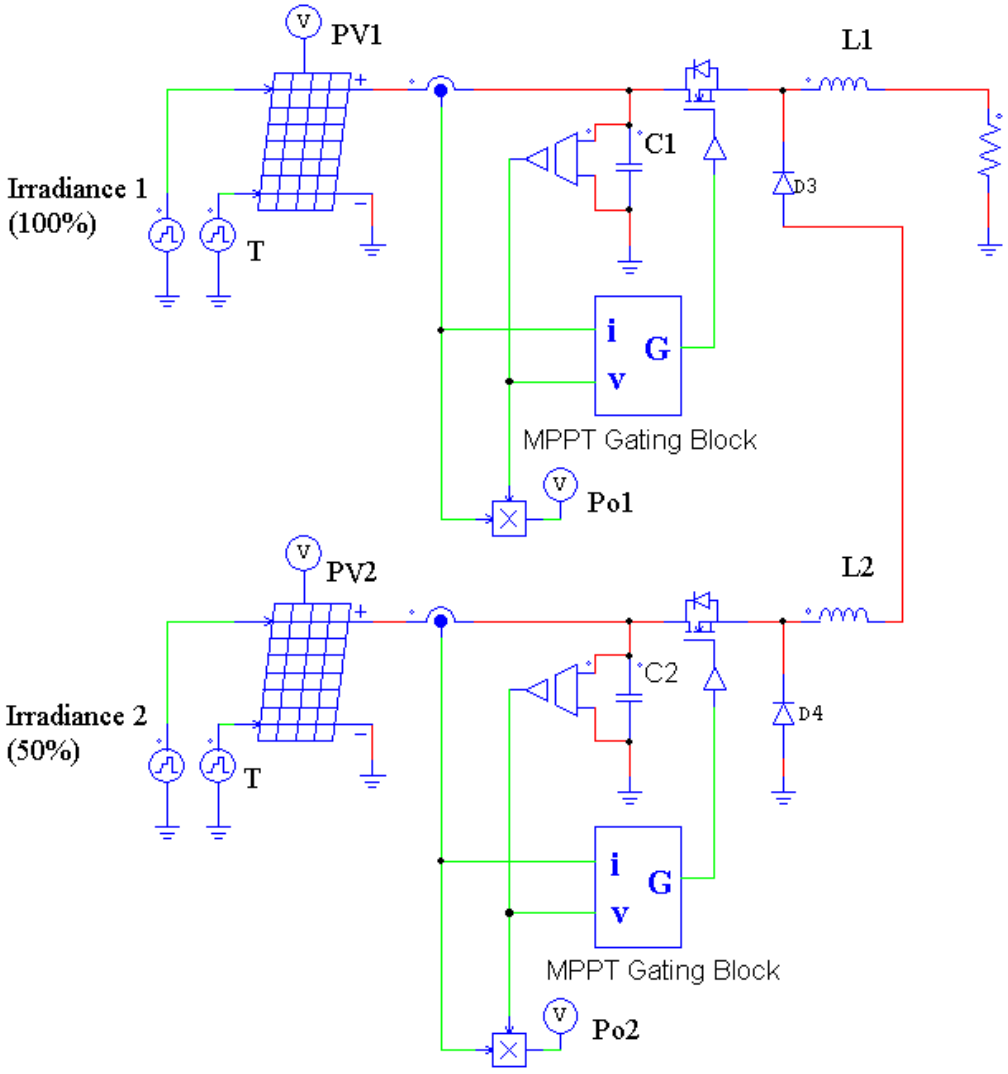

Fig. 4.23 (b) Two PV modules connected in series with uneven irradiance and independent MPPT block.

Table 4.3 Summary of simulated results for converter topology under partial shading Conditions

Sl. No	MPPT Algorithm	Maximum average power available at input of PV module 1 (W)	Maximum average power available at input of PV module 2 (W)	Average output Power of the PV System when the two PV modules were connected in series (W)	Average output Power of the PV System when the two PV modules are operated independently (W)
1	P & O algorithm	16.2	32.5	35.59	39.38
2	Variable Step Incremental algorithm	16.2	32.5	39.96	45.49
3	Proposed Hybrid Algorithm	16.2	32.5	41.39	47.24

The above concept of partial shading was extended to single phase AC photovoltaic system. In the proposed system there is no interconnection between PV modules, but there is interconnection between the associated DC–DC converters. Therefore, each PV module can operate at its own optimal power and current ensuring all the available energy in the PV array to be delivered. The irradiance data collected was converted into 100% and 50% insolation as shown as Case A and Case B of Fig. 4.24 to evaluate the performance of PV system under partial shading conditions.

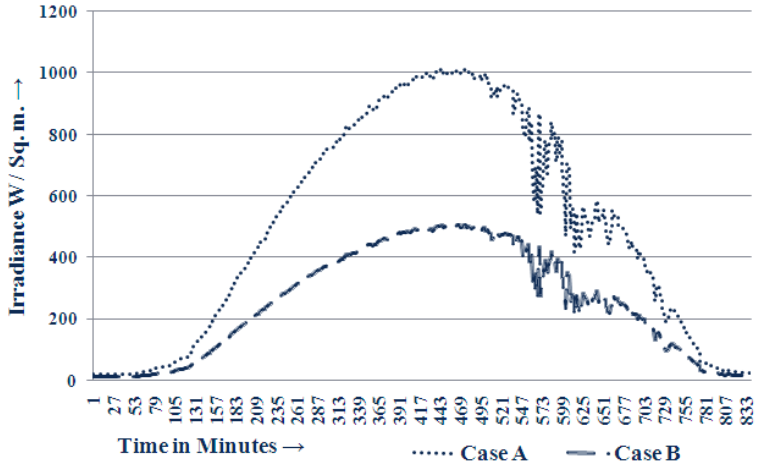

Fig. 4.24 The irradiance data collected for one day at city of Alandi, and extrapolated data for partial shading.

The insolation data of Fig. 4.24 were given to centralized inverter topology and

modular inverter topology through a stage of proposed MPPT and the DC-DC converter stage as shown in Fig. 4.25 and Fig. 4.26, respectively, for the Case A and Case B of insolation conditions to observe the effect of partial shading conditions on series connected PV modules.

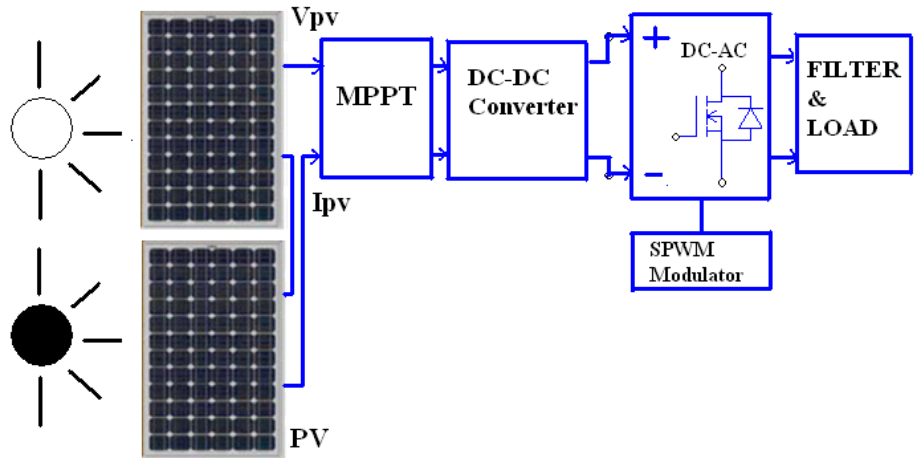

Fig. 4.25 Centralized inverter topology for multiple modules.

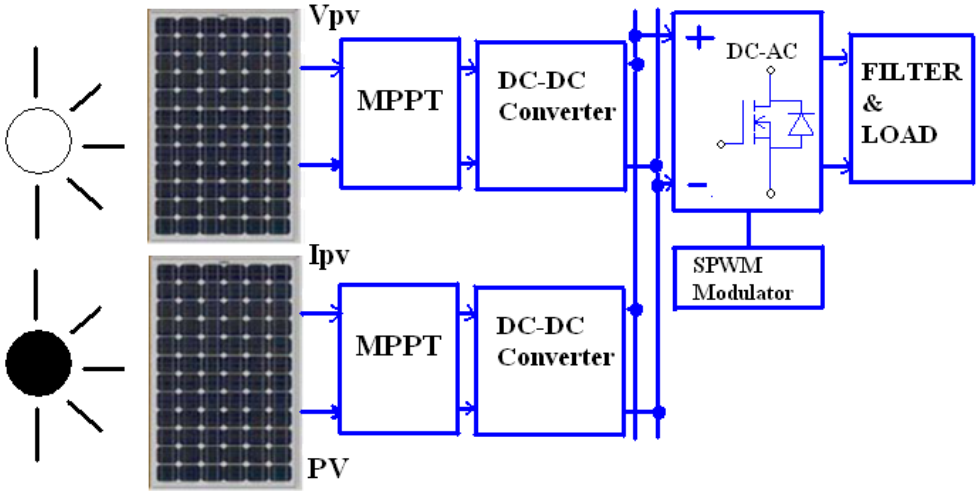

Fig. 4.26 Modular inverter topology for multiple modules.

The average output powers for the two inverter topologies with the proposed hybrid algorithms were evaluated. The observations have been summarized in Table 4.4. It is observed from the Table 4.4 that the P&O, variable step incremental algorithm and the proposed algorithm with modular inverter shows an improvement of 16.65%, 16.90 % and 17.63 %, respectively, for average power compared to centralized inverter topology (column-4) for partial shading conditions and the proposed algorithm shows an improvement of 5.89% and 1.49% as compared to P&O and variable step MPPT algorithms.

Table 4.4 Summary of simulated results for inverter topology under partial shading.

Sl. No	MPPT Algorithm	**Parameter**	**Average output power of centralized inverter topology (W)**	**Average output power of modular inverter topology (W)**
1	P & O algorithm	Case A	11.23	13.10
		Case B	13.10	13.10
2	Variable Step Incremental algorithm	Case A	12.13	14.18
		Case B	14.18	14.18
3	Proposed Hybrid Algorithm	Case A	12.59	14.81
		Case B	14.81	14.81

In Table 4.4, the Case A represents the study of two PV modules connected in series with an uneven illumination at full and 0 (W/m^2) insolation, and Case B represents the two PV modules connected in series with uniform illumination at half the insolation (W/m^2). The average power was calculated using Eq. (4.4) and listed in Table 4.4.

4.7 NEURO FUZZY CONTROLLER

The neural network and fuzzy controller are very accurate for non linear systems but are slow due to involvement of computational complexity. To overcome this drawback, an efficient Neuro-Fuzzy controller (NFC) for attaining MPPT of PV systems is proposed (Goudar et al. 2012a). The proposed NFC is the combination of FLC and ANN. The dataset for training of ANN is generated based on the fuzzy rules, so the network complexity is reduced. The efficiency of the proposed controller is enhanced by an evolutionary algorithm (EA). The EA optimize the power converter duty cycle and observes the array output of the PV system. The output of the EA is then applied to the NFC, and the MPPT of the PV system is determined. The EA is a subset of evolutionary computation, which is used for converging quickly to an operating point. In conventional algorithm, the optimization is based on the PV current and the corresponding power value. But in the present study, the optimization is based on the

change of PV current and change of power. So, the power loss and the time are reduced for obtaining the optimal solution.

4.7.1 Fuzzy Controller

The function of fuzzy controller is mainly based on fuzzy rules that are generated through fuzzy set theory. The fuzzy controller performs three processes: (i) fuzzification, (ii) decision making, and (iii) defuzzification. Fuzzification is the process of changing the crisp value into fuzzy value which has no fixed set of procedure and it is achieved by different types of fuzzifiers.

The shapes of fuzzy sets may be triangular, trapezoidal or other. A triangular fuzzy set is employed, the fuzzified output is subjected to the decision making process, which contains set of rules. By using the fuzzy rules, the change of current, change of power, and the corresponding converter output are determined. Finally, the defuzzification process is performed and the output of the fuzzy controller ΔC^F is obtained. The structure of designed FLC is shown in Fig. 4.27 and the steps involved in the design of FLC are given just below the figure.

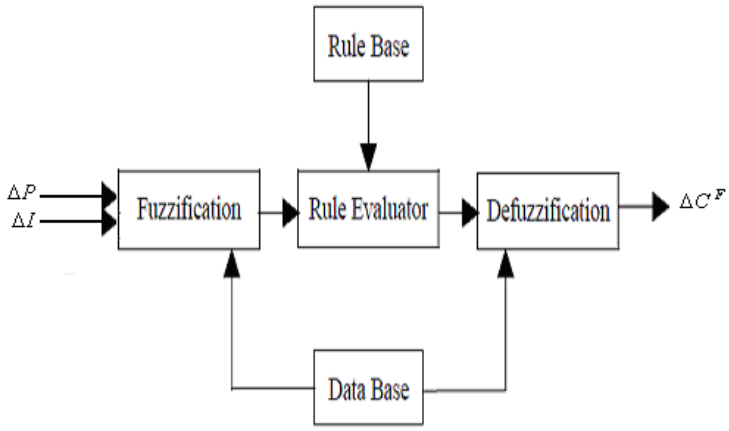

Fig. 4.27 Fuzzy controller structure for PV system.

- Choose the control variable for the power.
- Select the range of ΔP , ΔI and ΔC^F values of the system.
- Perform the fuzzification process.
- Design the decision making rules as per the selected range.
- Perform the defuzzification process.
- Evaluate the system output.

The ΔP and ΔI are the inputs for FLC, and the output is ΔC^F. The linguistic variables of the input and output of the fuzzy system are Negative Big, Negative Small, Positive Small, and Positive Big, which are referred as NB, NS, PS, and PB, respectively, in the rule base. The developed fuzzy rules are tabulated in Table 4.5. The ΔC^F is determined by means of fuzzy rules.

Table 4.5 Fuzzy rules for determining ΔC^F

ΔI \ ΔP	NB	NS	PS	PB
NB	PB	PS	NS	NB
NS	PB	PS	NS	NB
PS	NB	NS	PS	PB
PB	NB	NS	PS	PB

4.7.2 Neural Network

Neural Network (NN) is an artificial intelligence technique, used for generating training dataset, and testing the applied input data. A feed forward type NN is employed in the proposed method. Usually, NN is composed of three layers namely, input layer, hidden layer, and output layer. The input layer consist of two inputs, i.e., ΔP and ΔI and the output of the NN is network calculated voltage, which is represented by ΔC^{NN}. The process of NN is performed in the hidden layer. The structure of the network is illustrated in Fig. 4.28.

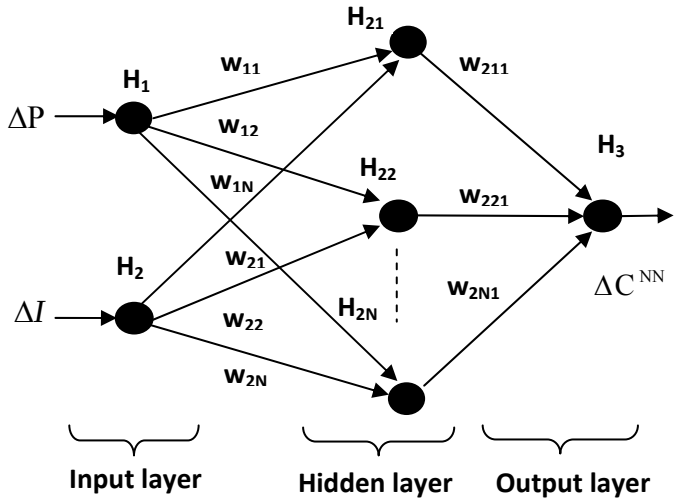

Fig. 4.28 Network structure of proposed system.

The hidden layer of the network is denoted as $H_{21}, H_{22}, \ldots\ldots\ldots H_{2N}$ and the weight of neuron is represented as w. The weight of neuron from input layer to hidden layer is w_1 and hidden layer to output layer is w_2. Here, the Back Propagation (BP) neural network training and weight adjustment are utilized.

4.7.3 N-F Controller

The proposed neuro-fuzzy (N-F) controller is the combination of fuzzy controller and neural network. The performance of hybridization is based on the mean operation. The converter output ΔC is determined from the output of the N-F controller. The converter output is determined using the following equation

$$\Delta C = \frac{1}{2}\left(\Delta C^{F} + \Delta C^{NN}\right) \tag{4.5}$$

where $\Delta C = \begin{bmatrix} \Delta C(1) \\ \Delta C(2) \\ : \\ : \\ \Delta C(t) \end{bmatrix}$, $\Delta C^{F} = \begin{bmatrix} \Delta C^{F}(1) \\ \Delta C^{F}(2) \\ : \\ : \\ \Delta C^{F}(t) \end{bmatrix}$

and $\Delta C^{NN} = \begin{bmatrix} \Delta C^{NN}(1) \\ \Delta C^{NN}(2) \\ : \\ : \\ \Delta C^{NN}(t) \end{bmatrix}$

ΔC^{F} is the fuzzy controller output and ΔC^{NN} is the neural network output. Using the Eq. (4.5), the maximum output of the converter is determined. The proposed MPPT algorithm based hybrid controller is implemented in MATLAB and simulink (Gilbert et al. 2008). The description of the PV module is given in Table. 4.6 and the plot of module current vs module voltage, and module power vs module voltage is shown in Fig. 4.29 (a) and Fig. 4.29 (b).

Table 4.6 Description of the PV module

Parameters		Range
PV Module	Short Circuit Current	5.2 A
	Open Circuit Voltage	22.0 V
	Maximum Power	78 W

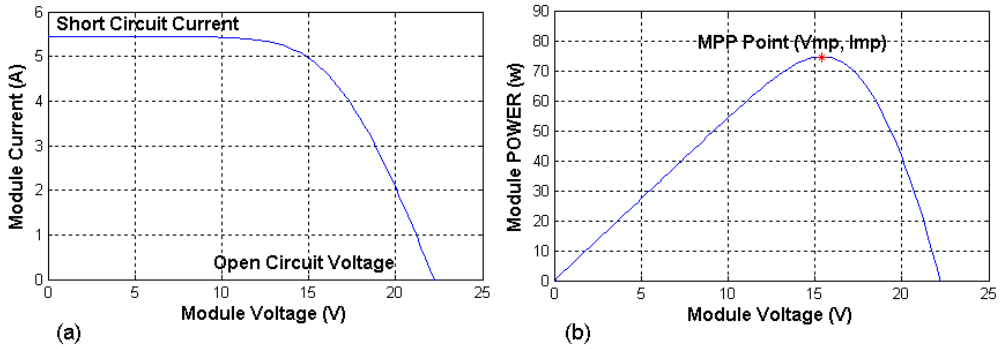

Fig. 4.29 (a) Module voltage vs current (b) Module voltage vs power characteristic curves.

The efficiency of the proposed controller is tested with PV system. The output performance of the proposed hybrid controller is compared with the fuzzy controller and neural network. The simulation model of the proposed controller based PV system is illustrated in Fig. 4.30.

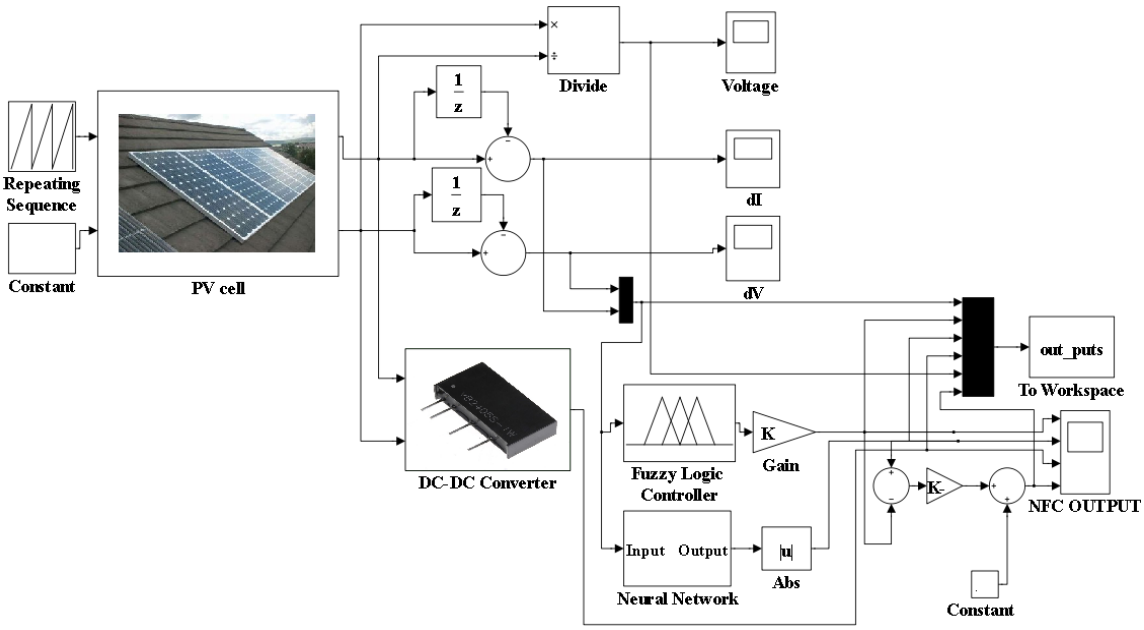

Fig. 4.30 Simulation model of hybrid controller based PV system.

The details of implementation of PV module and DC-DC converter are shown in Fig. 4.31 and Fig. 4.32. The output power characteristics of the proposed system are analyzed. The system output is analyzed for the current, voltage and the corresponding power values. The change in values are determined on the basis of current value and the previous value. The maximum converter output depends on the change of current and the change of power values.

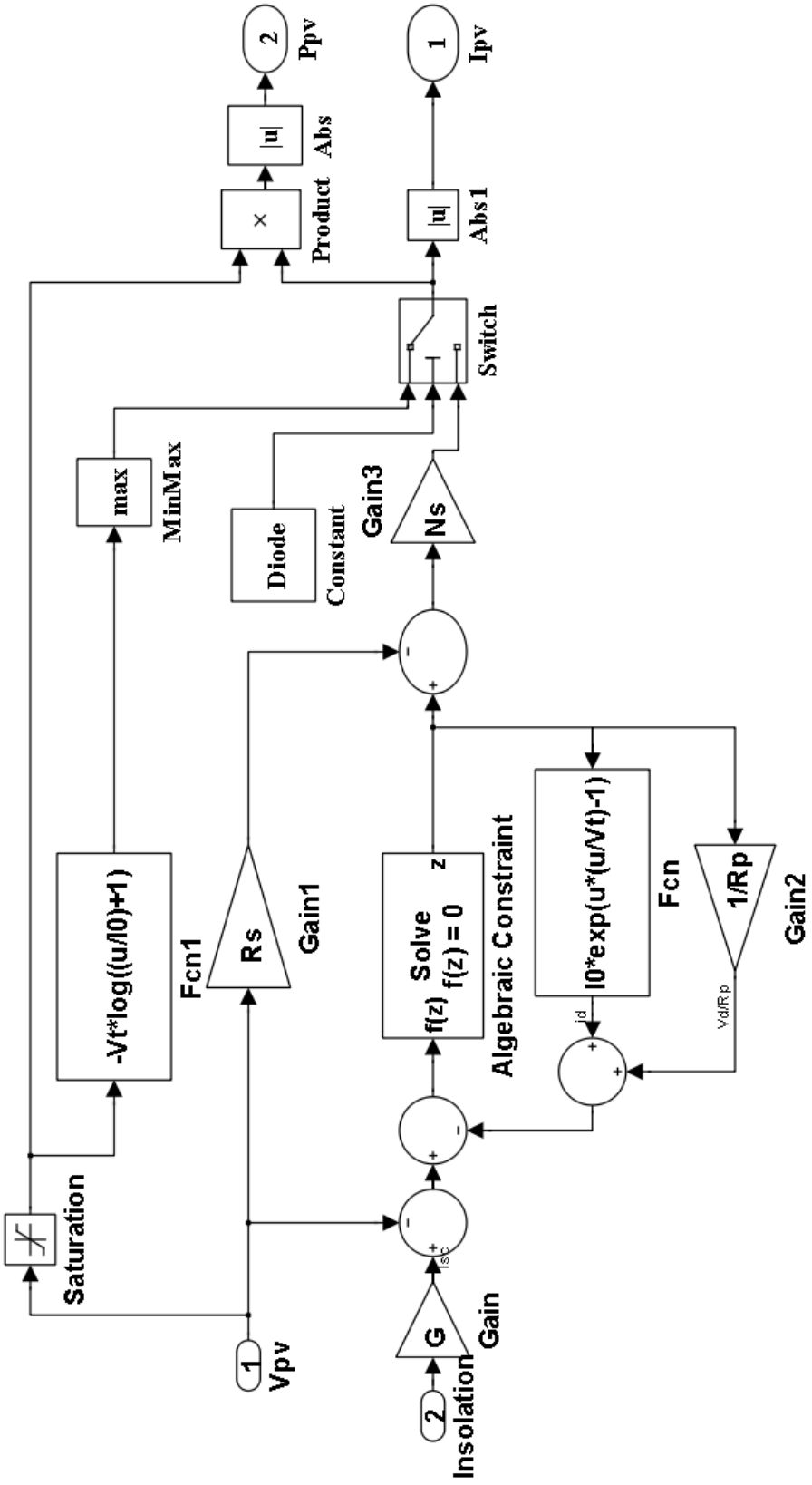

Fig. 4.31 Simulation model of PV cell.

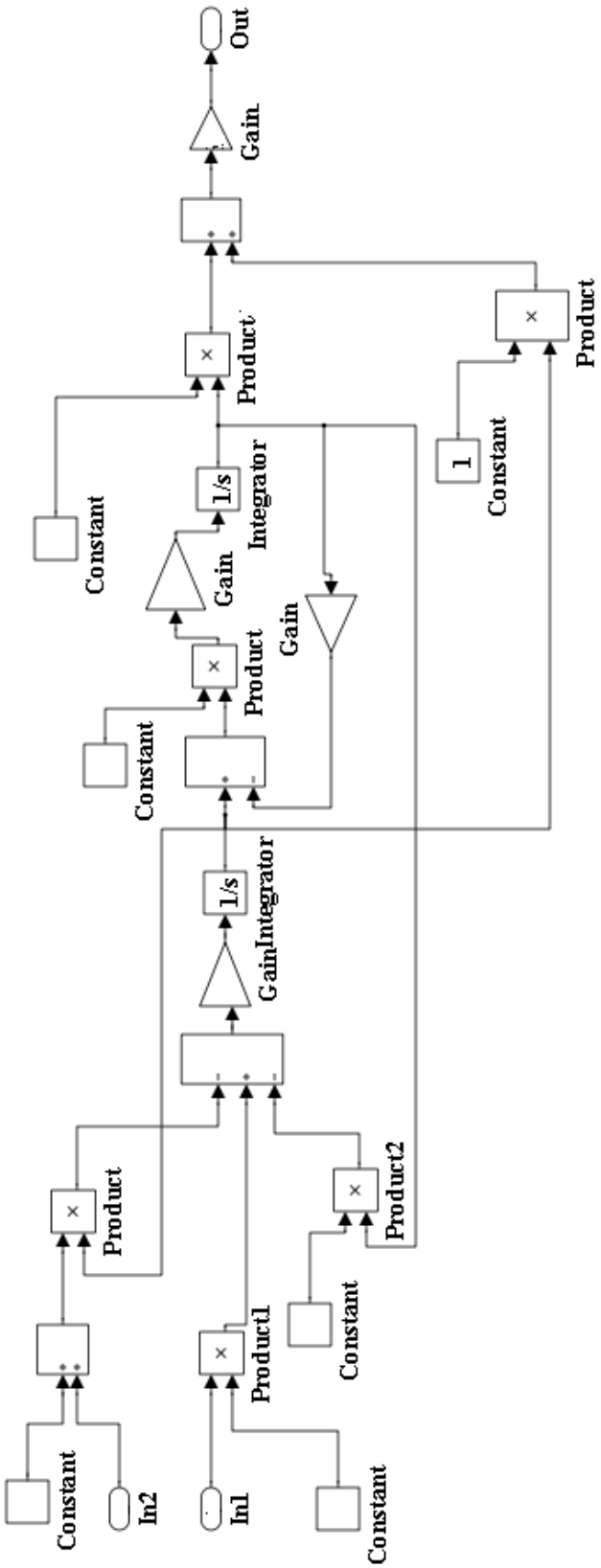

Fig. 4.32 Simulation model of DC-DC converter.

The fuzzy rules are generated with respect to the change of current, the change of voltage and the change of DC-DC converter output. The range of rules is defined for the values of parameter selected for implementation. The performance of the DC-DC converter output is analyzed at a different time instant and shown in Fig. 4.33.

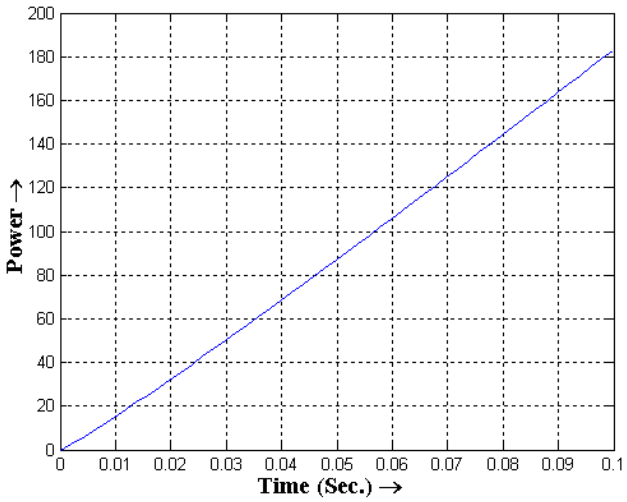

Fig. 4.33 Performance of DC-DC converter output.

For making maximum converter output, the enhanced hill climbing algorithm based hybrid controller is proposed. Using the proposed hill climbing algorithm, the change of current and the change of power are optimized at a different time. The optimized change of current and the change of power values are then applied to the input of the proposed hybrid controller. The performance of the change of current and the change of power with respect to time is described in Fig. 4.34 and Fig. 4.35, respectively.

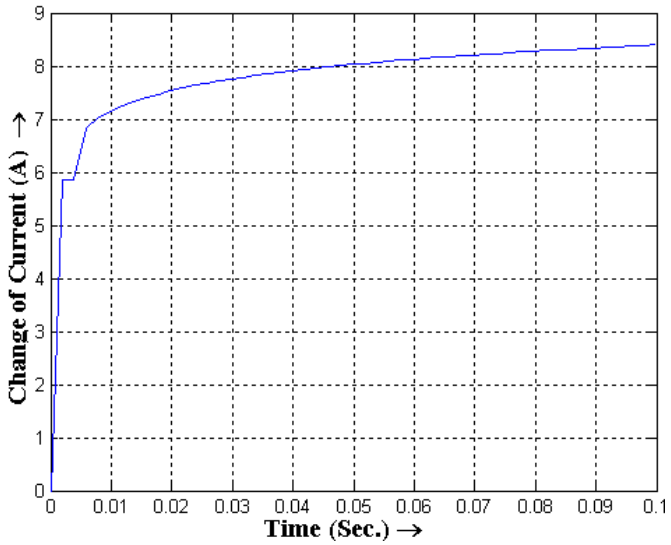

Fig. 4.34 Performance of change of current.

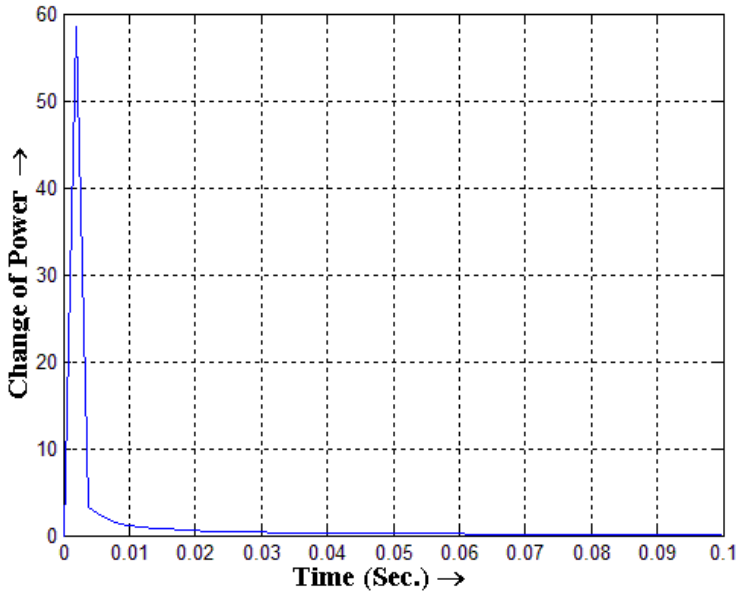

Fig. 4.35. Performance of change of power.

The fuzzy rules are generated with respect to the change of current, the change of voltage and the change of DC-DC converter output. The rules are defined on the basis of parameter values selected for the implementation. The membership function diagram of the change of current, the change of power and the converter output are illustrated in Fig. 4.36 (a), Fig. 4.36 (b) and Fig. 4.36 (c), respectively.

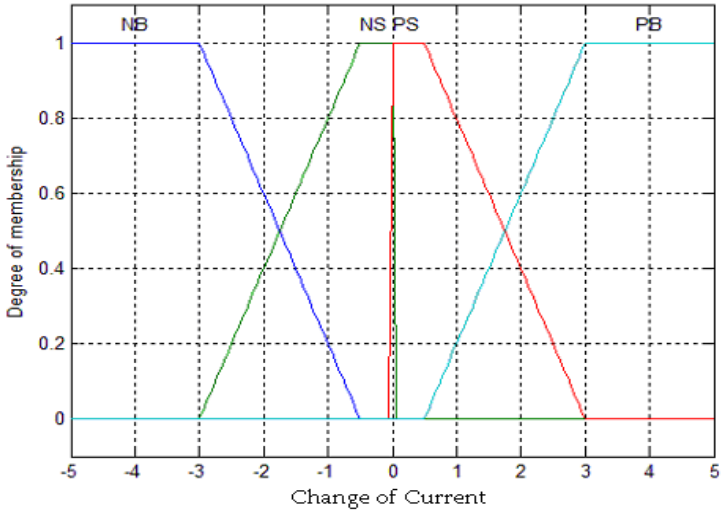

Fig. 4.36 (a) Membership function of change of current.

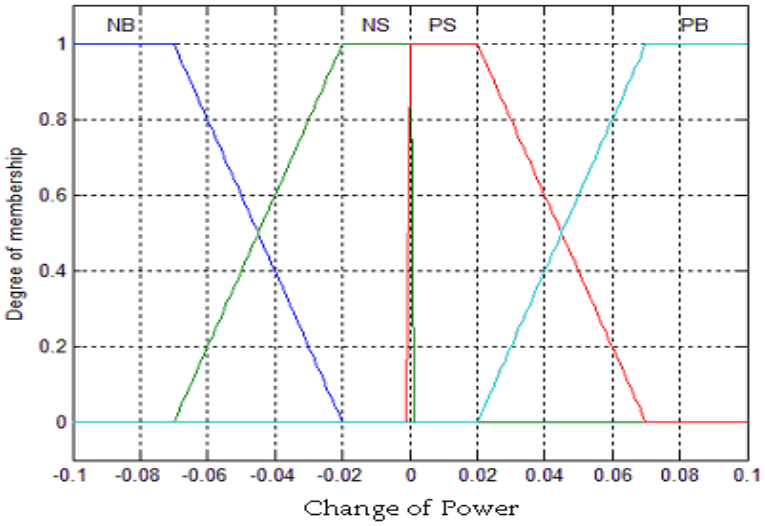

Fig. 4.36 (b) Membership function of change of power

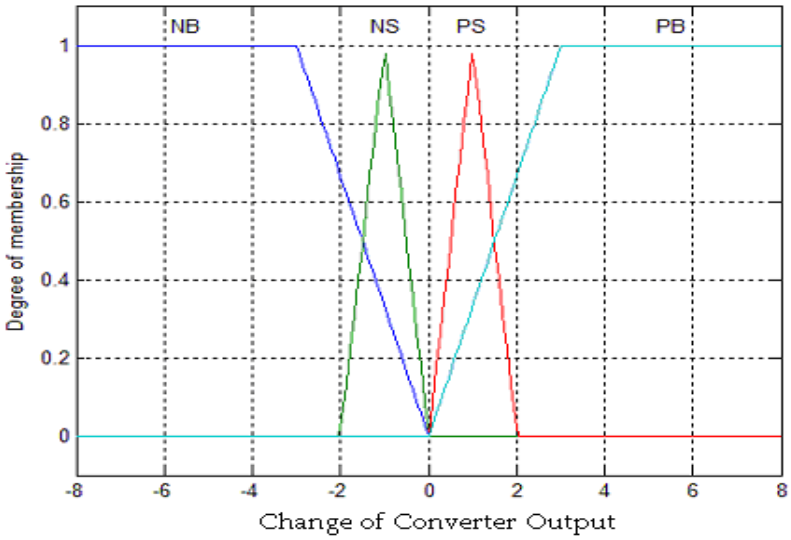

Fig. 4.36 (c) Membership function of change of converter output.

The 3-D structure of the fuzzy rules is shown in Fig. 4.37 and the output performance of the fuzzy controller in Fig. 4.38. The back propagation training error of the network for achieving the target of the system output is shown in Fig. 4.39.

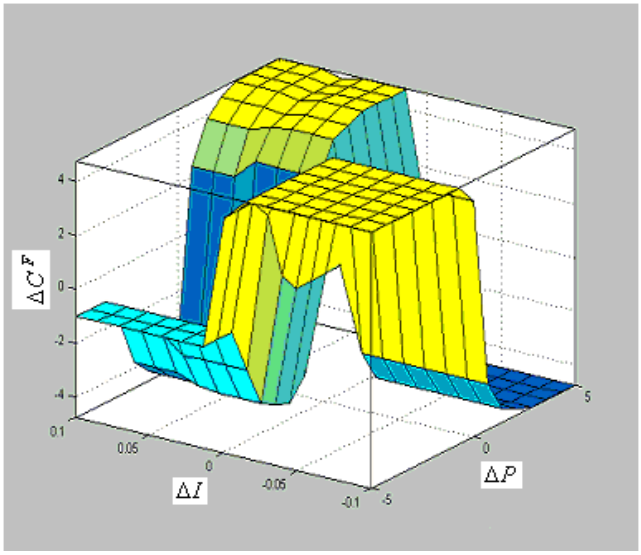

Fig. 4.37 Structure of input and output fuzzy rules.

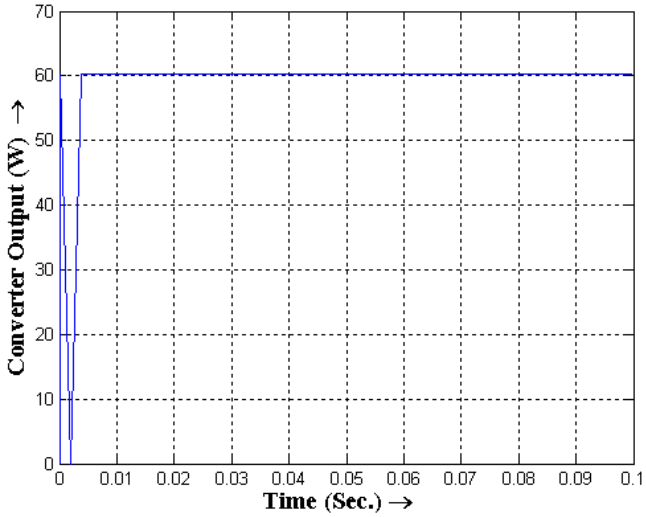

Fig. 4.38 Performance of fuzzy controller output.

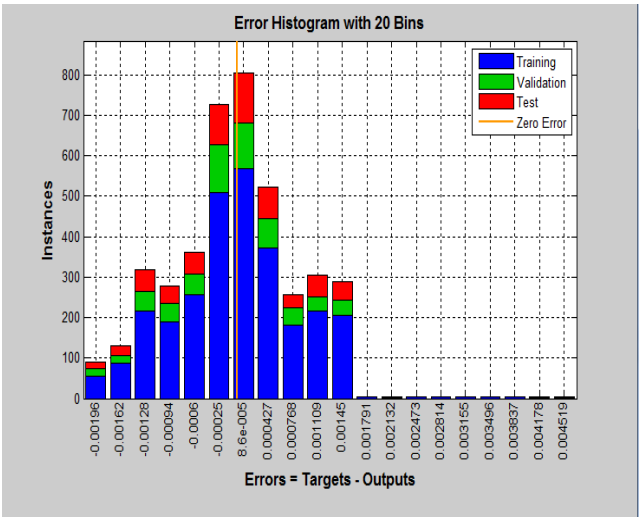

Fig. 4.39 Performance of network error histogram.

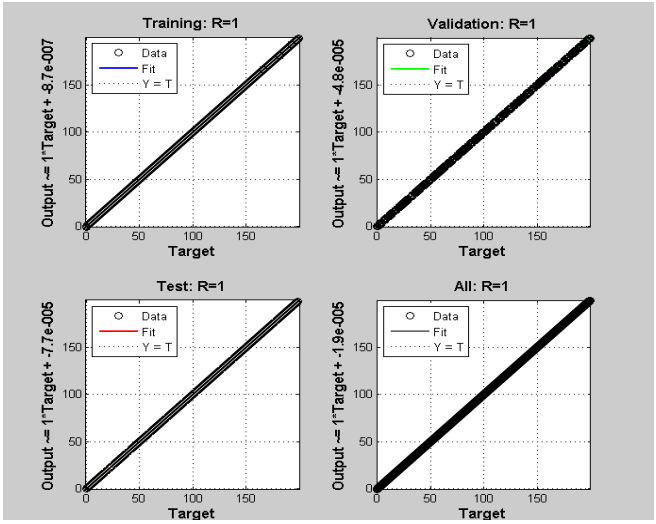

Fig. 4.40 (a) The network performance plots - Regression analysis.

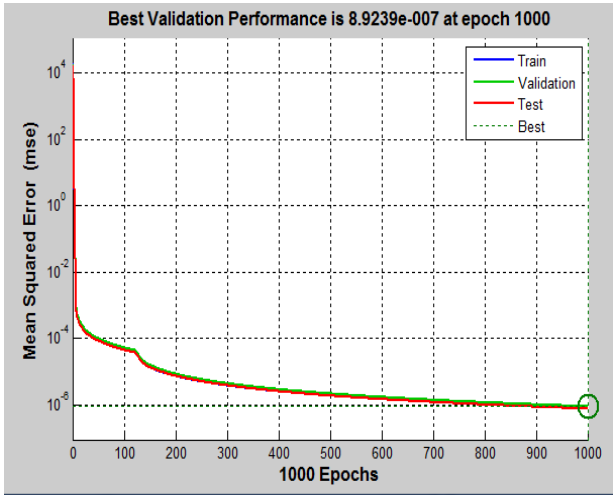

Fig. 4.40 (b) The network performance plots - Network validation performance.

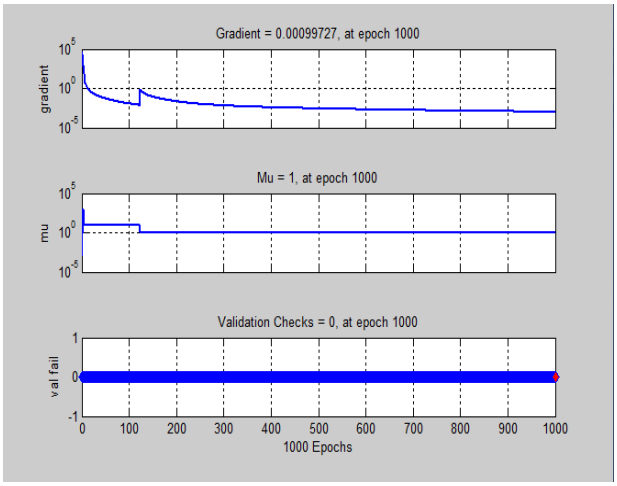

Fig. 4.40 (c) The network performance plots - Training state.

The neural network performance of regression, validation, and training state are shown in Figs. 4.40 (a), 4.40 (b) and 4.40 (c). The output performance of the neural network is analyzed and is shown in Fig. 4.41. Further, the outputs of the fuzzy controller and neural network are hybridized using mean operator and the N-F hybrid controller is developed. The performance of N-F controller is shown in Fig. 4.42. Finally, the output of the fuzzy controller, neural network and the neuro-fuzzy controller are compared and shown in Fig. 4.43.

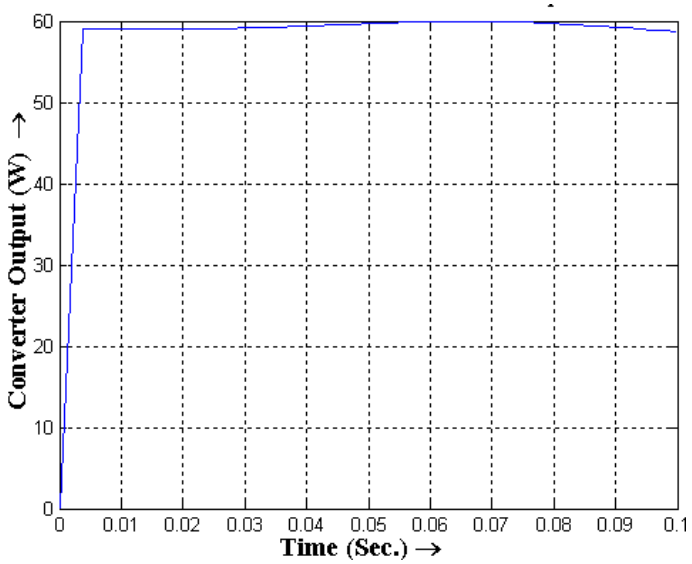

Fig. 4.41 Performance of neural network output.

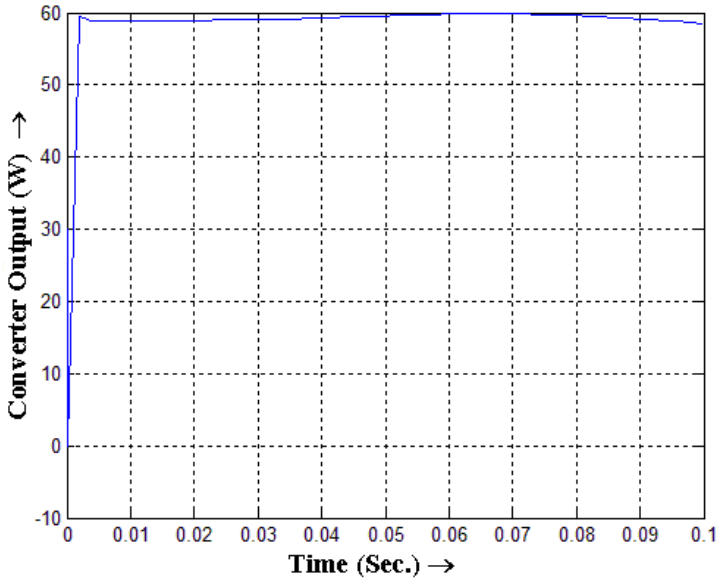

Fig. 4.42 Performance of neuro-fuzzy controller output.

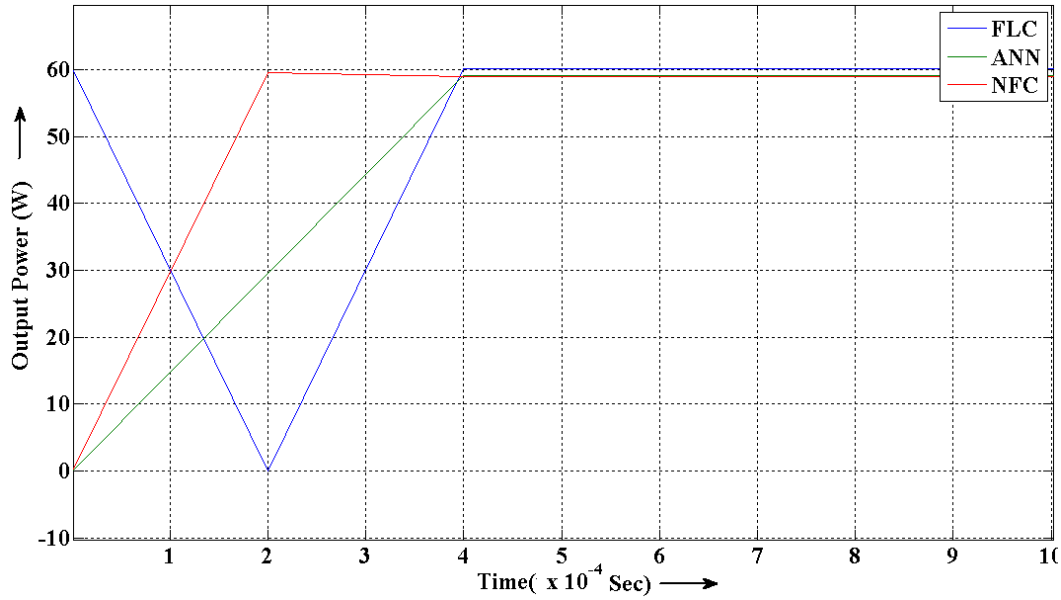

Fig. 4.43 Comparison performance of FLC, ANN and NFC.

The proposed neural network and fuzzy controller based hybrid controller has accurately reached the maximum power tracking point of PV system. However, the convergence time of the hybrid controller is less than the fuzzy and neural network based controllers.

4.8 DISCUSSION AND CONCLUSION

The proposed hybrid algorithm combines the advantages of FCV, variable step and optimized P&O algorithm. The changes in the environmental conditions are tracked by a more efficient variable step size with two different algorithms initiated for slowly varying environment conditions and fast varying environment conditions. In the proposed hybrid algorithm, it has been observed that the starting response time is improved by 140 ms and 54.57 ms, respectively, for the P&O and variable step incremental algorithms. The overall efficiency of 96.41% has been achieved with the proposed hybrid algorithm which demonstrates the soundness of the proposed method. The proposed hybrid algorithm has been tested for partial shading conditions. The simulations results show an improvement of 12.36%. Further, neuro-fuzzy controller (NFC) has been simulated using MATLAB and simulink controller, which is a combination of artificial neural network (ANN) and fuzzy logic controller (FLC). The simulated results of three are compared and an improvement of 2 ms has been observed in the starting characteristics of NFC and shown in Fig. 4.43.